Two-Mirror Compact System for Ideal Concentration of Diffuse Light

SHLOMI STEINBERG[1,*], NANDOR BOKOR[2], AND NIR DAVIDSON[3]

[1] Department of Computer Science, University of California, Santa Barbara, United States
[2] Department of Physics, Budapest University of Technology and Economics, 1111 Budapest, Budafoki u. 8
[3] Department of Physics of Complex Systems, Weizmann Institute of Science, Israel
[*] Corresponding author: p@shlomisteinberg.com

Compiled March 12, 2022

We introduce a simple, compact two-mirror system for diffuse light concentration. The design principle is based on local conservation of optical brightness. The system design is flexible, and we are able to compute mirror shapes given arbitrary incident beam direction and target cross-sectional shape. As illustration, we showcase our design for flat and cylindrical target geometries, and we also demonstrate that our system is able to concentrate efficiently along one or two dimensions. We perform numeric experiments that confirm our theoretical results and provide diffuse light concentration very close to the thermodynamic limit in all cases we considered.

http://dx.doi.org/10.1364/ao.XX.XXXXXX

1. INTRODUCTION

Diffused light concentrators have been considered for solar energy concentration [1–3], light collection for instruments [4–6] and efficient light coupling into fiber optics [7]. Ideal concentration is limited to the *thermodynamic limit*, which arises from the conservation of optical brightness [8]. Widely-used concentrators rely on a simple parabolic mirror (PM). The performance of such a concentrator is worse by factors of 2 or π, for flat and cylindrical targets, respectively, in two dimensions, and by a factor of 4 in three dimensions, compared with the thermodynamic limit [9]. Compound parabolic concentrators (CPCs) are non-imaging concentrators whose performance can approach the thermodynamic limit [8]. However, CPCs, when used alone, tend to be large, as their length-to-width ratio scales as $\sim 1/\sin\left(\frac{\epsilon}{2}\right)$, where ϵ is the full diffusivity angle of the incident light (for direct solar light $\sin(\epsilon) \approx 0.01$).

Concentrators made of curved diffractive optical elements were shown to provide compact ideal concentration [4]. However, such systems are limited to quasi-monochromatic radiation and typically suffer from lower efficiency. Using multi-element reflective concentrators, it is possible to design compact non-imaging concentrators [10]. Recently, a reflective three-mirror system was purposed that approaches the thermodynamic limit in two dimensions by using a coordinate transformer to spatially shape the diffusivity of the incident illumination [9]. This system is compact, however, the three-mirror system lacks axial symmetry, and the use of three successive reflections for each ray introduces losses. In addition, when working as a three-dimensional concentrator, this design required successive five mirrors, introducing even higher losses.

In this paper we propose two-mirror concentratores (2MC) for diffused light that approach the thermodynamic limit. Our system is compact, axially symmetric, and is suitable to broadband light. As two-dimensional concentrators (concentration along one direction) and for small incoming diffusivities they achieve ideal concentration at the thermodynamic limit, and their performance remains close to ideal even for larger diffusivities. When applied as three-dimensional concentrators (concentration along two directions), concentration close to the thermodynamic limit is still achieved with only two mirrors. For simplicity, we assume mirrors with perfect (100%) reflectances. However, finite mirror reflectances can be readily incorporated in our design.

This paper is organized as follows: In Section 2 we present a new analytic design principle for two-mirror diffuse light concentrators, based on local conservation of the optical brightness. We apply it to one-side flat targets in two and three dimensions and to cylindrical target and study its performance characteristics and discuss analytic results in Section 3, and conclude in Section 4.

Throughout the paper we use a somewhat different terminology than several others working in the field. To avoid confusion, here we give a list of concepts that we use in the paper, with their alternatives, often used by others, written in square brackets: diffused light concentrator [nonimaging concentrator], phase-space volume [étendue], (local) conservation of optical brightness [(local) convervation of étendue], diffusivity [angular extent].

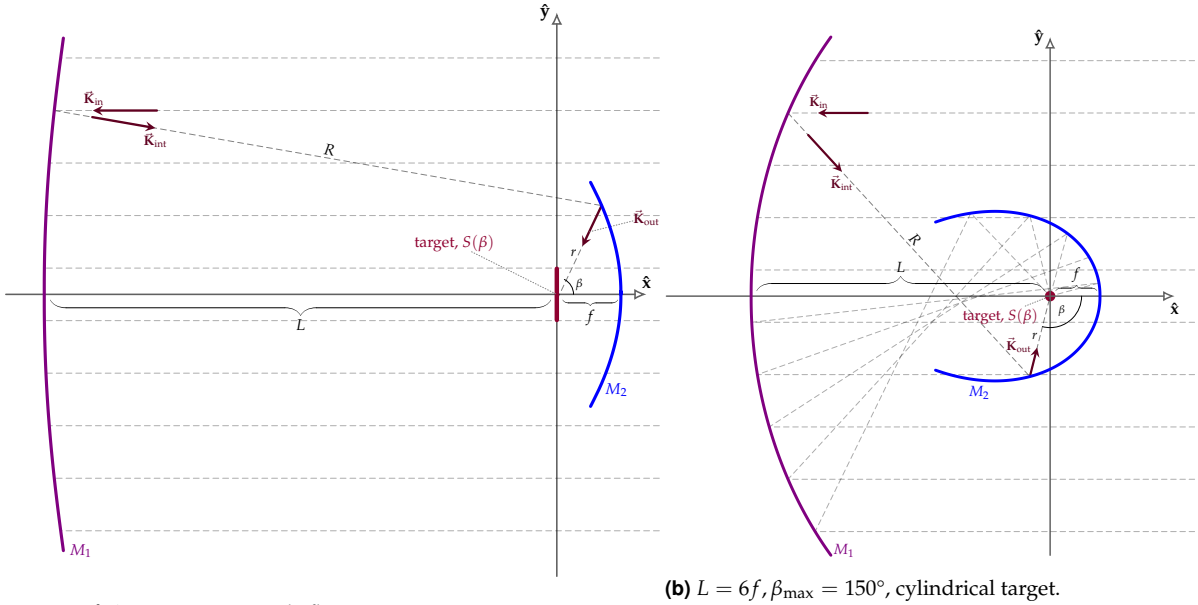

(a) $L = 8f, \beta_{max} = 80°$, one-side flat target.

(b) $L = 6f, \beta_{max} = 150°$, cylindrical target.

Fig. 1. Schematics of 2-mirror concentration (2MC) system setups and notation. On-axis concentration is performed along the y-direction. Mirror shapes obtained by integrating Eqs. (7) and (11) from $\beta = 0°$ to β_{max} for incoming light with uniform intensity $I(y) = constant$ and uniform diffuse angle and requiring $S(\beta) = \cos\beta$ for the flat target $S(\beta) \equiv 1$ for the cylindrical target.

2. DESIGN

The brightness of a diffuse beam is defined as the encircled energy divided by (four-dimensional) phase-space volume [2]. Thus in the ray optics picture local brightness can be thought of as the local phase-space density (PSD) of rays. According to the thermodynamic limit of brightness conservation, the greatest PSD of rays at the output of a diffuse light concentrator cannot be larger than the greatest PSD at the input. If the input beam has uniform PSD, such as sunlight, the thermodynamic limit implies that optimal concentration cannot be reached unless the output beam at the target has uniform PSD too [11]. Conventional focusing elements such as a PM lead to highly nonuniform PSDs in their focal region. This can be intuitively understood if we consider that light cones hitting a PM farther from its symmetry axis travel a larger distance to the focus and expand to larger spot sizes than light cones that travel closer to the optical axis. This property of PMs thus limit their concentration performance to well below the thermodynamic limit [9]. We propose to overcome this limitation by a two-mirror system that manipulates the incoming diffuse illumination so that light cones hitting the second mirror farther from the target become narrower than light cones hitting the second mirror closer to the target, and exactly compensate for the increased distance, so as to form a focal spot with the minimum size allowed by the thermodynamic limit. The principle that enables us to manipulate local diffusivities along the beam cross-section is local conservation of PSD [2, 4]. Previously, we proposed a three-mirror concentrator [9] that consists of a cascade of two mirrors performing an optical coordinate transformation and an additional parabolic mirror that performs focusing. In the present paper we improve that design to consist only of two mirrors which together perform the combined task of coordinate transformation and concentration. As will be shown below, our design leads to a device which, when illuminated with an input beam with uniform PSD, leads to a uniform PSD of rays on the target, and thus achieves optimal concentration at the thermodynamic limit.

The schematics of our "two-dimensional" design (concentration along a single axis) are shown in Fig. 1a for a one-side flat target, and Fig. 1b for a cylindrical target (e.g., sunlight on a pipe). The optical axis is $\hat{\mathbf{x}}$ and concentration is performed on the xy-plane onto a target centered around $(0,0)$. Note that Fig. 1b shows a so-called "inverting" design where rays originating from the top of mirror 1 hit the bottom of mirror 2 and vice versa. We chose this geometry for the cylindrical target, because it leads to significantly less shadowing by mirror 2 compared with the "non-inverting" design (Fig. 1a).

The two-mirror system performs an intensity transformation [12] from the incident beam to the output beam $I(y) \to S(\beta)$, where $\beta(y)$ is the desired angular incident direction to the target (chosen in Section 3 to ensure maximal concentration for a given target geometry). The shapes of the two mirrors are now analytically calculated via ray tracing to provide this transformation and to focus the central incoming rays onto the center of the target $(0,0)$. The incident beam direction $\vec{\mathbf{K}}_{in}$ is chosen a priori. For an on-axis design, as illustrated in Fig. 1, $\vec{\mathbf{K}}_{in} = (-1,0)$. Let (x,y) and (x',y') be the positions on the mirrors. Initially, for an incident ray at $y = 0$, we set $x = -L$, $x' = f$ and $y = y' = 0$, where the given constants L and f are the distance from the focal point to the first mirror and the focal distance of the second mirror, respectively. The intermediate and outgoing ray directions are then

$$\vec{\mathbf{K}}_{int} = \tfrac{1}{R}(x' - x, y' - y)\,, \tag{1}$$

$$\vec{\mathbf{K}}_{out} = -\tfrac{1}{r}(x', y')\,, \tag{2}$$

with $R = |(x,y) - (x',y')|$ and $r = |(x',y')|$. The mirrors' normals are dictated by the law of reflection:

$$\vec{\mathbf{n}}_1 = \vec{\mathbf{K}}_{\text{int}} - \vec{\mathbf{K}}_{\text{in}} = \left(\frac{x'-x}{R} + 1, \frac{y'-y}{R}\right), \tag{3}$$

$$\vec{\mathbf{n}}_2 = \vec{\mathbf{K}}_{\text{out}} - \vec{\mathbf{K}}_{\text{int}} = -\left(\frac{x'}{r} + \frac{x'-x}{R}, \frac{y'}{r} + \frac{y'-y}{R}\right). \tag{4}$$

By Fermat's principle it follows that $-x + R + r \equiv \text{const}$, i.e. the path lengths travelled by the different rays and focused to the same point are the same constant, and that constant must be $2L + 2f$ (the distance travelled by the $y \equiv 0$ ray). The slope of the first mirror can be written as:

$$\frac{\mathrm{d}x}{\mathrm{d}y} = -\frac{(\vec{\mathbf{n}}_1)_y}{(\vec{\mathbf{n}}_1)_x} = -\frac{y'-y}{x'-x+R} = -\frac{y'-y}{x'-r+2L+2f}, \tag{5}$$

and, by writing $(x', y') = r(\cos\beta, \sin\beta)$, we arrive at the differential equation:

$$\frac{\mathrm{d}x}{\mathrm{d}y} = \frac{y - r\sin\beta}{r\cos\beta - r + 2L + 2f}. \tag{6}$$

The desired angular intensity distribution $S(\beta)$ should match the Lambertian reflectance of the target to ensure local conservation of optical brightness. For a flat target we get $S(\beta) = \cos\beta$ and for a cylindrical target $S \equiv 1$ [9]. Using the local energy conservation, viz. $\mathrm{d}y\, I(y) = \mathrm{d}\beta\, S(\beta)$, solve for $y(\beta)$ and substitute it into Eq. (6), yielding:

$$\frac{\mathrm{d}x(\beta)}{\mathrm{d}\beta} = \frac{\mathrm{d}y(\beta)}{\mathrm{d}\beta}\frac{y(\beta) - r(\beta)\sin\beta}{r(\beta)(\cos\beta - 1) + 2L + 2f}, \tag{7}$$

where we made explicit the fact that r is a function of β.

Similarly, the slope of the second mirror becomes

$$\begin{aligned}\frac{\mathrm{d}x'}{\mathrm{d}y'} &= -\frac{(\vec{\mathbf{n}}_2)_y}{(\vec{\mathbf{n}}_2)_x} = -\frac{(r+R)\sin\beta - y}{(r+R)\cos\beta - x} \\ &= \frac{y - (r+R)\sin\beta}{(r+R)(\cos\beta - 1) + 2L + 2f}.\end{aligned} \tag{8}$$

Take the derivative of x' and y' with respect to β:

$$\frac{\mathrm{d}x'}{\mathrm{d}\beta} = \frac{\mathrm{d}r}{\mathrm{d}\beta}\cos\beta - r\sin\beta, \quad \frac{\mathrm{d}y'}{\mathrm{d}\beta} = \frac{\mathrm{d}r}{\mathrm{d}\beta}\sin\beta + r\cos\beta, \tag{9}$$

and substitute the above into the left-hand side of Eq. (8), yielding

$$\frac{\frac{\mathrm{d}r}{\mathrm{d}\beta} - r\tan\beta}{\frac{\mathrm{d}r}{\mathrm{d}\beta}\tan\beta + r} = \frac{y - (r+R)\sin\beta}{(r+R)(\cos\beta - 1) + 2L + 2f}. \tag{10}$$

Simplifying and noting again the explicit dependence on β produces the differential equation

$$\frac{\mathrm{d}r(\beta)}{\mathrm{d}\beta} = r(\beta)\frac{(r(\beta)+d)\sin\beta - y(\beta)\cos\beta}{(r(\beta)+d)\cos\beta + y(\beta)\sin\beta - r(\beta) - R}, \tag{11}$$

with $d = R - 2f - 2L$.

Eqs. (7) and (11) couple the shape of mirror 1, $x(\beta)$, to the shape of mirror 2, $r(\beta)$, and are integrated numerically from $\beta = 0°$ to a chosen $\beta_{\max}$ for given $L, f, S(\beta)$, and $I(y)$.

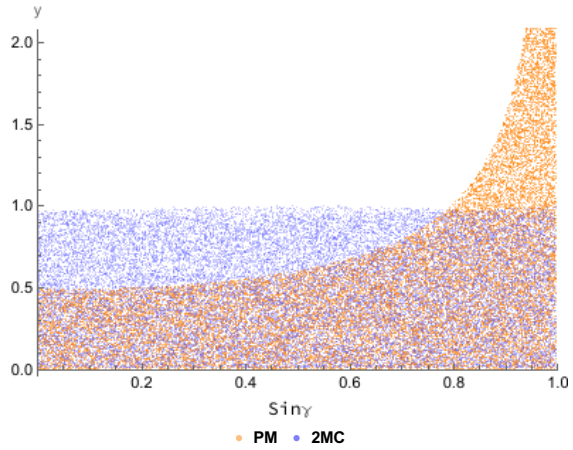

Fig. 2. Phase-space hit plot, concentration along one dimension, $\epsilon = 0.01$. Flat target, $L = 20f, \beta_{\max} = 80°$. The computed 2MC target length is $0.2f$. y is the normalised position on the flat target (such that $y = 0$ is at the center of the flat target and $y = 1$ is at one of the edges), γ is the angle between the target's normal and the incident ray.

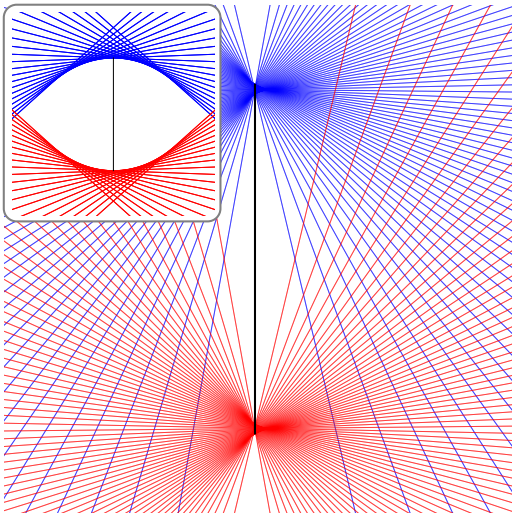

Fig. 3. Focal region of flat target, concentration along one dimension, $L = 20f, \beta_{\max} = 85°, \epsilon = 0.01$. Shown are extreme incoming edge rays, with incidence angle of $+\frac{\epsilon}{2}$ (red) and $-\frac{\epsilon}{2}$ (blue). (inset) Ray traces for the PM with $\beta_{\max} = 45°$, with optimal target shown in black (note, the inset has a different $\beta_{\max}$ compared to Fig. 2, as large $\beta_{\max}$ admit far larger caustics which are hard to visualize).

3. RESULTS

A. Concentration Along One Dimension: Flat Target

We first consider two-dimensional concentration on a one-side flat target (elongated along z) as in Fig. 1a with $S(\beta) = \cos\beta$ and $\beta_{\max} < 90°$. We assume an incoming light with uniform intensity $I(y) = \textit{constant}$ and uniform diffuse angle and numerically integrate Eqs. (7) and (11) for on-axis geometry to obtain the mirror shapes. We performed Monte Carlo ray-tracing simulations to compute the concentration performance and quantitatively compare our 2-mirror concentrator (2MC) to the single parabolic mirror (PM). The simulations were performed by ray tracing a

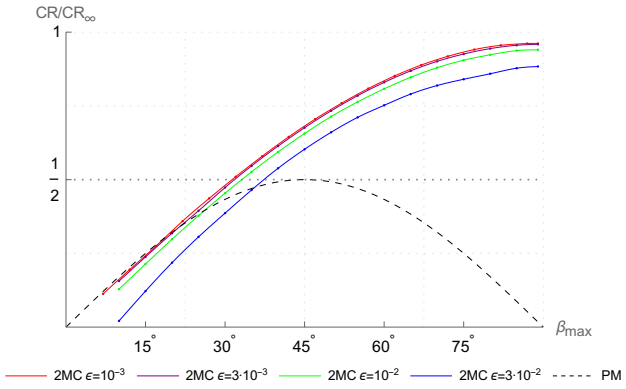

Fig. 4. Normalized concentration ratio NCR for concentration along one dimension on a flat target with $L = 20f$ as a function of the maximal angular incident direction to the target $\beta_{\max}$, for different values of the incoming diffusive angle ϵ. PM is an analytic plot of $\sin\beta\cos\beta$ for the NCR of the parabolic mirror.

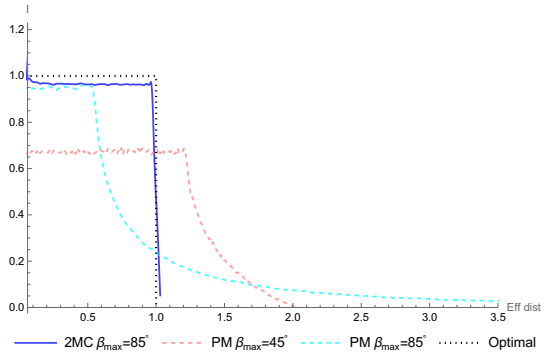

Fig. 5. Intensity distribution for concentration along one dimension on a flat target, $L = 20f, \epsilon = 0.01$.

large number of rays (8192), randomly oriented with the incident angle uniformly distributed on $[-\frac{\epsilon}{2}, +\frac{\epsilon}{2}]$.

Fig. 2 presents the calculated phase space diagram of all rays hitting the target. As seen, The 2MC generates uniform distribution of rays both in position and in angle, enabling optimal concentration, whereas the PM produces a highly non-uniform phase-space distribution of rays with a long tails, that prevent optimal concentration.

An image of the caustics of the 2MC at the vicinity of the geometrical focal point, Fig. 3, was generated by tracing only the extreme incoming edge rays, with incidence angle of $+\frac{\epsilon}{2}$ (red) and $-\frac{\epsilon}{2}$ (blue). While the caustics of the 2MC trace the edges of the flat target (satisfying the so-called "edge ray principle" [2]), the caustics produced by the PM (inset) admit significant deviations.

Next, we evaluate the minimal target size A needed to contain all concentrated rays. The non-zero diffusivity of the incident illumination induces a small spatial shift of the optimal target position from the theoretic focal point. To find the optimal target shift, we perform ray-tracing simulations and numerical gradient descent optimization. The optimal shift, possibly originating from field curvature, is found to be a small fraction of the target size and grows quadratically with ϵ. From the target size A and the lateral size of the incoming beam D we find the concentration ratio $\mathrm{CR} = \frac{D}{A}$ and the normalized concentration ratio $NCR = \mathrm{CR}/\mathrm{CR}_\infty$, where the thermodynamic limit for diffuse light concentration is $\mathrm{CR}_\infty = \frac{1}{\sin(\epsilon/2)}$, i.e. for small ϵ, $CR_\infty \approx \frac{1}{\epsilon/2}$.

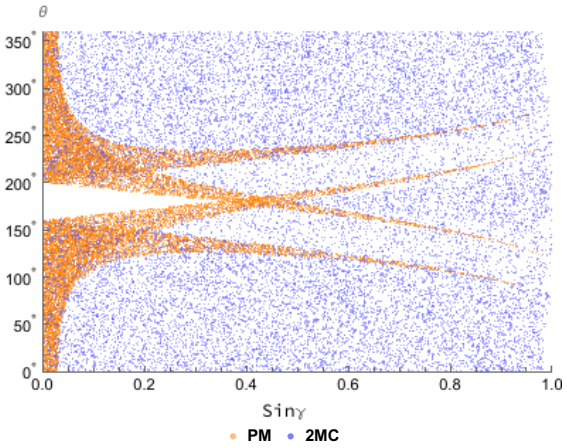

Fig. 6. Phase-space hit plot, concentration along one dimension on an optimal cylindrical target, $L = 50f, \beta_{\max} = 160°$, $\epsilon = 0.01$. The computed radius of the 2MC target is $0.0505f$. θ is the position on the cylindrical target, γ is the angle between the target's normal and the incident ray. Note that the optimal target sizes differ between the 2MC and the PM. Also note that $\theta = 0$ points in the $+\hat{\mathbf{x}}$ direction for the 2MC and in the $-\hat{\mathbf{x}}$ direction for the PM, that is $\theta = 0$ always aligns with $\beta_{\max} = 0$.

Fig. 4 presents NCR as a function of $\beta_{\max}$ for several values of ϵ for our 2MC and the single PM concentrators. While a single PM reaches only 50% of the thermodynamic limit for any value of ϵ [9], our 2MC design reaches a near ideal NCR of 0.96 at $\beta_{\max} = 88°$ for small incoming diffusivity $\epsilon = 0.001$ and only slightly worse at larger values up to $\epsilon = 0.03$. The near ideal concentration of the 2MC is also manifested in the calculated intensity distributions on the target, presented in Fig. 5. As seen, the 2MC generates flat intensity distribution nearly identical to the ideal concentration (dashed line) whereas the PM generates nonuniform distributions exceeding the ideal target size by a factor of 2 for its optimal $\beta_{\max} = 45°$ and by even more at larger value of $\beta_{\max}$.

The "non-inverting" 2MC with $L = 20f$ and at $\beta_{\max} = 89°$ produces about 21.8% shadowing for the on-axis design. We applied our design method to several additional configuration of 2-mirror concentration onto a flat target. We obtained very similar results to those presented in this section for other values of L/f and also for an off-axis 2-mirror configuration where shadowing is completely avoided.

B. Concentration Along One Dimension: Cylindrical Target

Next, we apply our design to a cylindrical target elongated along z (for example, sunlight concentrated onto a water pipe) as in Fig. 1b with $S(\beta) = 1$ and $\beta_{\max} < 180°$. We assume again incoming light with uniform intensity $I(y) = constant$ and uniform diffuse angle and numerically integrate Eqs. (7) and (11) for on-axis geometry to obtain the mirror shapes.

Fig. 6 presents the calculated phase space diagram of all rays hitting the cylindrical target. As seen, The 2MC generates the desired near-uniform distribution of rays both in position and in angle, compared with the highly non-uniform distribution of the PM.

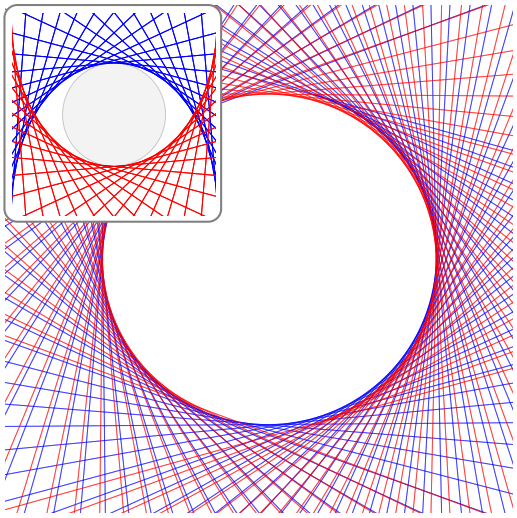

Fig. 7. Focal region of 2MC setup for cylindrical target, concentration along one dimension, $L = 50f, \beta_{\max} = 165°, \epsilon = 0.01$. Shown are extreme incoming edge rays, with incidence angle of $+\frac{\epsilon}{2}$ (red) and $-\frac{\epsilon}{2}$ (blue). (inset) Ray traces for the PM with $\beta_{\max} = 90°$, with optimal target in gray (note, the $\beta_{\max}$ is different in the inset compared to Fig. 6, for visualization purposes).

A caustics image generated by ray tracing the extreme rays, displayed in Fig. 7, indicate near perfect concentration by our 2MC system, while the caustic image for the PM (inset) shows significant aberrations that impair the performance of the PM concentrator for the same target.

The calculated normalized concentration of our 2MC system, compared to that of the PM concentrator, is presented in Fig. 8. As seen NCR reaches for our 2MC 0.937 at $\beta_{\max} = 172.5°$ for small incoming diffusivity $\epsilon = 0.001$ and slightly lower for $\epsilon = 0.03$, whereas the PM reached a maximal $NCR = \frac{1}{\pi}$ at $\beta_{\max} = 90°$. The generated "inverting" 2-mirror system with $L = 50f$ and at $\beta_{\max} = 170°$ results in 8.6% shadowing for the on-axis design. We obtained similar results for other values of L/f and also for the off-axis configuration where shadowing is completely suppressed.

C. Concentration Along Two Dimensions: Flat Circular Target

Due to its symmetry around the incidence plane (the xy plane which contains the incidence vector $\vec{\mathbf{K}}_{\text{in}}$), our on-axis design naturally applies also to three-dimensional concentrators by simply replacing y with radius in cylindrical symmetry and testing it with 3D ray tracing. In the three-dimensional case, the theoretical concentration performance limit of the PM is $NCR = \frac{1}{4}$ of the thermodynamic limit, both for a flat and ball target [9]. Our 2MC design achieves $NCR = 0.91$ for $L = 20f$, $\beta_{\max} = 80°$ on a flat circular target, see Fig. 9. The shadowing produced by the "non-inverting" and "inverting" designs are 2.6% and 0.3%, respectively. We believe that the cylindrical symmetry of our design is an important factor in reducing the impact of skew rays [4, 8] on the system's performance. This enables us to achieve good three-dimensional concentration performance, greatly surpassing the performance of our previous design [9]. The good performance of the 2MC system when concentrating along two dimensions may be attributed to axial symmetry as well as the fact that rays always travel an almost constant

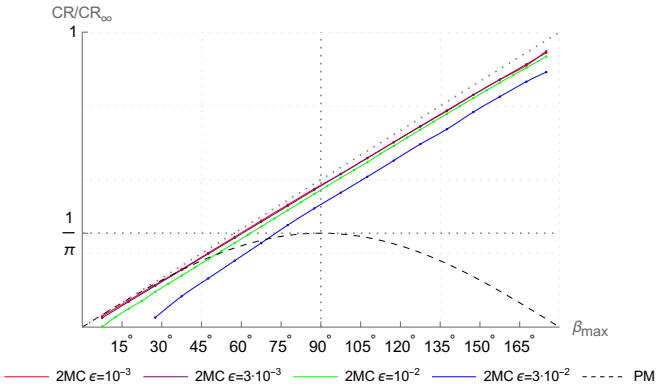

Fig. 8. Normalized concentration ratio NCR for concentration along one dimension on a cylindrical target, $L = 50f$ as a function of the maximal angular incident direction to the target $\beta_{\max}$, for different values of the incoming diffusive angle ϵ. PM is an analytic plot of $\frac{1}{\pi}\sin\beta$ for parabolic mirror.

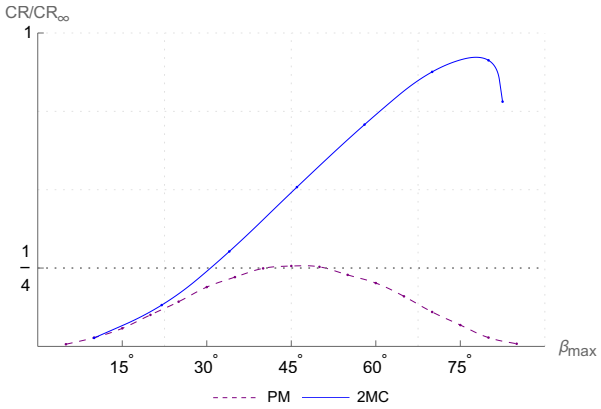

Fig. 9. Normalized concentration ratio NCR for concentration along two dimensions on a circular flat target, $L = 20f, \epsilon = 0.01$. PM are analytic plots of $\sin^2\beta\cos^2\beta$ for parabolic mirror.

distance inside the 2-mirror system, see Fig. 10.

4. DISCUSSION AND CONCLUSION

We presented a new design for a compact two-mirror system for diffuse light concentration. We numerically analyzed the performance of this system, and demonstrated two-dimensional concentration approaching the thermodynamic limit for both flat and cylindrical targets for small incoming diffusivity ϵ and excellent performance also in three dimensional concentration where the deleterious effect of skew rays is reduced by our symmetric and compact design.

As ϵ increases, the optimal target position shifts slightly away from the focal centre. We employ numeric gradient descent to find a locally optimal shift, which in some cases significantly improves the performance even for large ϵ. The length of our 2MC system is comparable to the incident beam's lateral size D (as seen in Fig. 1) and is independent of ϵ, in contrast to a CPC whose length scales as D/ϵ making it much shorter for small ϵ (such as direct solar light).

Our design principle is simple, analytic and flexible and can be extended to additional target shapes and geometry, off-axis configuration to alleviate shadowing effects, diffuse light sources

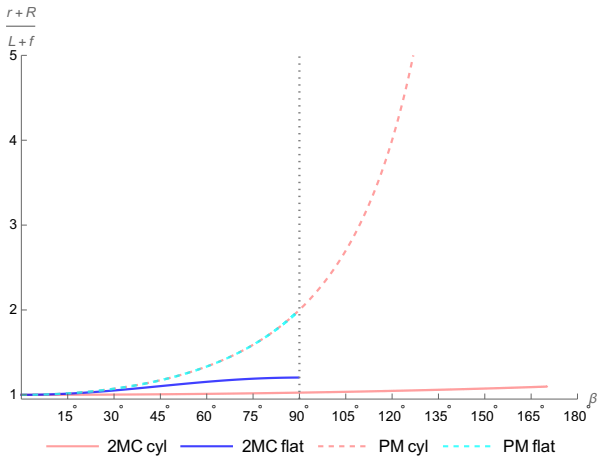

Fig. 10. Normalized travel distances $\frac{r+R}{L+f}$ (see Fig. 1) of a concentrated ray as a function of its β are nearly constant for the two-mirror concentrates, and sharply increase with β for the parabolic mirror .

at finite distances or with nonuniform intensity and diffusivity.

It is interesting to compare our design with existing compact concentrator designs, such as the multi-element reflective/refractive concentrators [10]. Both our design and [10] have similar length-to-width ratios, similar performances (approaching ideal concentration at small ϵ and reduced performance as ϵ increases), high total transmission, minimal number of reflections, and no contact with the receiver. However, while [10] relies on the edge ray principle [1] yielding rather complex calculations of the aspheric optical surfaces, our design uses the central rays together with local conservation of brightness which provides simpler, more intuitive and more flexible designs.

Since our design provides local conservation of optical brightness, optical reciprocity ensures that our ideal 2MC system onto some target shape can be used in reverse as an ideal collimator for diffuse light sources of the same shapes. Such an ideal collimator will preserve the brightness of the source upon collimation and moreover will generate uniform intensity and diffusivity. The design can be readily generalized for any desired nonuniform intensity or diffusivity of the collimated beam.

Finally, we note that although our design imposes local conservation of brightness by only considering the path of the central rays without explicitly constraining the other rays, it does provide imaging conditions of the diffuse source (i.e. all rays emerging from any point on the diffuse source are focused onto a single point on the flat target). This intriguing result is closely related to the aplanatic conditions for aberration-free imaging [13] which emerges from the local conservation of brightness [3], and paves the way for numerous applications for our design for imaging systems free of first-order aberrations.

5. ACKNOWLEDGMENTS

We would like to thank Pofessor Jeffrey M. Gordon from the Ben-Gurion University of the Negev, Israel, for illuminating discussions.

6. DISCLOSURES

The authors declare no conflicts of interest.

REFERENCES

1. I. Bassett, W. Welford, and R. Winston, *III Nonimaging Optics for Flux Concentration* (Elsevier BV, 1989).
2. R. Winston, J. C. Minano, P. G. Benitez, W. contributions by Narkis Shatz, and J. C. Bortz, *Nonimaging Optics* (2005).
3. J. Gordon, "Aplanatic optics for solar concentration," Opt. Express **18**, A41–A52 (2010).
4. N. Bokor and N. Davidson, "Ideal collimation, concentration, and imaging with curved diffractive optical elements," Rev. Sci. Instruments **76**, 111101 (2005).
5. N. Davidson, L. Khaykovich, and E. Hasman, "High-resolution spectrometry for diffuse light by use of anamorphic concentration," Opt. Lett. **24**, 1835 (1999).
6. S. Yamaguchi, T. Kobayashi, Y. Saito, and K. Chiba, "Collimation of emissions from a high-power multistripe laser-diode bar with multiprism array coupling and focusing to a small spot," Opt. Lett. **20**, 898 (1995).
7. H. Zbinden and J. E. Balmer, "Q-switched nd:ylf laser end pumped by a diode-laser bar," Opt. Lett. **15**, 1014 (1990).
8. W. Welford and R. Winston, *High Collection Nonimaging Optics* (Elsevier BV, 1989).
9. N. Bokor, K. Jahn, and N. Davidson, "Compact reflective system for ideal imaging concentration," Appl. Opt. **58**, 485 (2019).
10. J. C. Miñano and J. C. González, "New method of design of nonimaging concentrators," Appl. Opt. **31**, 3051 (1992).
11. N. Davidson and N. Bokor, "Curved diffractive optical element for uniform concentration at the thermodynamic limit at finite distance," J. Opt. Soc. Am. A **21**, 656 (2004).
12. N. Davidson, A. A. Friesem, and E. Hasman, "Reflective and refractive systems for general two-dimensional beam transformations," Appl. Opt. **33**, 815 (1994).
13. D. Lynden-Bell, "Exact optics: a unification of optical telescope design," Mon. Notices Royal Astron. Soc. **334**, 787–796 (2002).